Dyes and Pigments 194 (2021) 109614

Contents lists available at ScienceDirect

Dyes and Pigments

journal homepage: www.elsevier.com/locate/dyepig

A sensitive and selective fluorescence probe for the detection of superoxide radical anion in vivo based on a protection-deprotection process

Liyan Chen [a,*], Xin Lu [a], Fengping Xiao [a], Di Wu [b,**]

[a] CCNU-uOttawa Joint Research Centre, Key Laboratory of Pesticides & Chemical Biology Ministry of Education, College of Chemistry, Central China Normal University, Wuhan, 430079, China
[b] School of Chemistry, Chemical Engineering and Life Science, Wuhan University of Technology, Wuhan, 430070, China

ARTICLE INFO

Keywords:
Superoxide radical anion
Fluorescent detection
Protection-deprotection strategy
Coumarin
Bioimaging

ABSTRACT

Superoxide radical anion ($O_2^{\cdot-}$) plays vital roles in numerous physiological and pathological processes. Thus, it is in great demand to develop an efficient fluorescence probe for the measurement of $O_2^{\cdot-}$. In the investigation, a new fluorescence probe NAP-SCM was developed for detection of $O_2^{\cdot-}$ on the basis of a protection-deprotection process. This probe, which utilizes coumarin as the fluorescent platform and 1,8-naphthalimidesulfonyl as the masking moiety, could monitor $O_2^{\cdot-}$ with good specificity, rapid response and low detection limit. More importantly, probe NAP-SCM displayed negligible cytotoxicity, good bio-compatibility and excellent capability of tracking the endogenous superoxide radical anion in live cells and live animals. The favorable observations illustrated that this probe has the promising potential to provide a valuable support for exploring the role(s) played by $O_2^{\cdot-}$ in the biologically functional processes.

1. Introduction

Reactive oxygen species (ROS) including superoxide radical anion ($O_2^{\cdot-}$), singlet oxygen ($^1O_2$), hypochlorous acid/hypochlorite (HOCl/$^-$OCl), hydrogen peroxide (H_2O_2) and hydroxyl radical (•OH) play important roles in cell signaling and homeostasis, such as pathogen response, aging and anti-inflammation regulation [1–3]. Among them, $O_2^{\cdot-}$ has received special attention because it is acted as the major precursor of many ROS and can be functioned as the marker for early ROS generation [4,5]. In addition, as a well-known mediator in oxidative chain reaction, $O_2^{\cdot-}$ involves in numerous pathologies such as intercellular signaling and non-specific immunity against bacteria, viruses and parasites [6–8]. However, a large amount of evidences indicate that the excessive generation of $O_2^{\cdot-}$ will lead to many photoreceptor cell damage and oxidative-stress-induced diseases including inflammation, autoimmune disorders, neurodegeneration and ischemia-reperfusion injury in surgery [9–12]. Therefore, it is critically meaningful to develop an efficient analytical method with high sensitivity and selectivity to monitor $O_2^{\cdot-}$ in vitro and in vivo.

To date, various analytical technologies have been applied to recognize the level of $O_2^{\cdot-}$, such as mass spectrometry (MS), high performance liquid chromatography (HPLC), electrochemical sensors, electron paramagnetic resonance (EPR) and several optical methods [13–17]. Though effective, there are still limitations existed. For example, electrochemical sensors and HPLC could recognize $O_2^{\cdot-}$ with high specificity, but they are complicated to fabricated. EPR and MS suffer the expensive instrument and only suitable for the detection of extracellular $O_2^{\cdot-}$. In contrast, fluorescent imaging technology becomes a vital method for the measurement of $O_2^{\cdot-}$ because of its high sensitivity, good selectivity and powerful potential for biological research [18–22]. During the past several years, a variety of elegant fluorescent probes have been implemented to detect $O_2^{\cdot-}$ via redox mechanism using hydroethidine (HE) and its mitochondria-targeting analogue (Mito-HE or MitoSOX) [23–26]. However, HE and its analogue are easy to be interfered by other intracellular species like Fe^{2+}, ascorbic acid and glutathione, resulting in the limitation of applications in bioimaging. In order to improve the degree of specificity for $O_2^{\cdot-}$, a series of fluorescence probes on the basis of protection-deprotection mechanism have been developed utilizing 2,4-dinitrobenzenesulfonyl [27–30], 4,5-dimethoxy-2-nitro-phenylsulfonyl [31], trifluoromethanesulfonyl [32–34] or diphenyl phosphinyl [35–40] as the representative reactive moieties. Though available, there is still plenty of room to improve such as the

* Corresponding author. .
** Corresponding author. .
E-mail addresses: clyan@mail.ccnu.edu.cn (L. Chen), chemwd@whut.edu.cn (D. Wu).

https://doi.org/10.1016/j.dyepig.2021.109614
Received 16 May 2021; Received in revised form 21 June 2021; Accepted 28 June 2021
Available online 29 June 2021

problems of high detection limit, complicated synthetic pathway, poor narrow linear, water-solubility and long reaction time. In this sense, more efforts should be made in constructing efficient fluorescent probes with novel masking moiety for the detection and imaging of $O_2^{\cdot-}$ in the living systems.

In the investigation described below, we would like to present a fluorescence probe for the detection of $O_2^{\cdot-}$ on the basis of a protection-deprotection process. The probe is constructed by the incorporation of 7-hydroxycoumarin platform and 1,8-naphthalimidesulfonyl unit. The novel masking moiety 1,8-naphthalimidesulfonyl unit is served for $O_2^{\cdot-}$ detection via protection-deprotection mechanism. We proposed that $O_2^{\cdot-}$ could induce the cleavage of S–O band and release the strong fluorescence emitted by 7-hydroxycoumarin (**HYCA**) (Scheme 1).

2. Experimental section

2.1. Reagents and instruments

All chemicals were obtained from commercial sources and used as received. ^{1}H NMR and ^{13}C NMR spectra were recorded using a Bruker 600 MHz instrument. Chemical shifts are expressed in ppm using tetramethylsilane as an internal reference, and coupling constants (J) are reported in Hz. High-resolution mass spectra were obtained via a Milli-Q water system (Agilent, USA). Fluorescence emission spectra were recorded using a fluorescence spectrophotometer (Agilent Cary Eclipse, USA). UV absorption spectra were conducted from an UV–Vis spectrophotometer (Agilent Cary 60, USA). Fluorescent images were acquired on laser confocal microscope (Leica TCS SP8X), and 50% of laser power was applied. All spectroscopic experiments were performed in a 1 × 1 cm quartz cell. Deionized water was used to prepare all aqueous solutions.

2.2. Preparation of reactive analytes

Superoxide radical anion solution ($O_2^{\cdot-}$) was prepared by adding KO_2 to dry dimethylsulfoxide. Hypochlorous acid (HOCl) was prepared by dilution of a 10% NaOCl solution in deionized water. Hydrogen peroxide (H_2O_2) was generated by dilution of a 28% solution in deionized water. Nitric oxide (NO•) was generated from SNP (sodium nitroferricyanide (III) dihydrate). $ONOO^-$ was prepared using the reported procedure and the concentration is confirmed using extinction co-efficient of 1670 $cm^{-1}M^{-1}$ at 302 nm in 0.1 M sodium hydroxide aqueous solutions [41]. Hydroxyl radical (•OH) was generated by mixing the solution of ammonium iron (II) sulfate (100 μM) and H_2O_2 in deionized water. Singlet oxygen ($^1O_2$) was generated by mixing H_2O_2 stock solution with 10 equivalents of HOCl. NO_2^- and hydrogen sulfide (H_2S) were generated by adding $NaNO_2$ and Na_2S to deionized water, respectively.

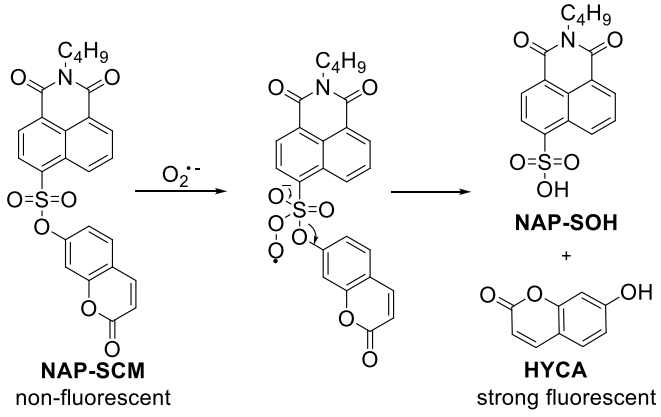

Scheme 1. Proposed reaction mechanism of probe **NAP-SCM** and $O_2^{\cdot-}$.

Glutathione (GSH), cysteine (Cys), homocysteine (Hcy), hydroquinone (HQ) and ascrobic acid (AA) were prepared by adding relative chemicals to deionized water.

2.3. Cell-culture

The macrophage cell line murine (RAW 264.7) were plated on the surface of a glass slide in Dulbecco's Modified Eagle Medium (DMEM) supplemented with penicillin (100 units/mL), 10% heat-inactivated Fetal Bovine Serum (FBS) and streptomycin (100 μg/mL). The cells were maintained in a humidified atmosphere of 5% CO_2/air at 37 °C.

2.4. Bioimaging in live cells and zebrafish

For confocal microscopy experiments of control experiment, RAW 264.7 cells or 72 h post-fertilization zebrafish were treated with probe **NAP-SCM** (10 μM) for 30 min, washed with DPBS. The experiments for monitoring endogenous superoxide radical anion, RAW 264.7 cells or zebrafish were treated with PMA (1 μg/mL) for 12 h or LPS (5 μg/mL) for 8 h, washed with DPBS buffer and then treated with probe **NAP-SCM** (10 μM) for 30 min. For a blocking experiment, cells or zebrafish were pre-cultured with Tiron (100 μM) for 1 h, then loaded with PMA or LPS, washed with DPBS buffer and then treated with probe **NAP- SCM** (10 μM) for 30 min. Images were collected at 465–495 nm with an excitation wavelength of 405 nm using a confocal imaging system.

2.5. Synthesis of intermediate NAP-SOK

The commercially available 4-potassiosulfo-1,8-naphthalenedicarboxylic anhydride (632 mg, 2.0 mmol) was added to 30 mL anhydrous ethanol under N_2 atmosphere and then *n*-butylamine (176 mg, 2.4 mmol) was added. The mixture was heated to reflux and vigorously stirred overnight. The reaction was cooled to room temperature and the ethanol was evaporated. The residue was washed with cold ethanol for several times and used for the next step without further purification.

2.6. Synthesis of probe NAP-SCM

The intermediate **NAP-SOK** (371 mg, 1.0 mmol) was dissolved in 20 mL $SOCl_2$ under nitrogen atmosphere. Then three drops of DMF were added to the mixture as the catalyst. The reaction was heated to reflux for 12 h. Then the solvent was evaporated under reduced pressure to obtain the yellow solid for the next step. The commercially available 7-hydroxycoumarin (162 mg, 1.0 mmol) was dissolved in 20 mL anhydrous THF under nitrogen atmosphere followed by the addition of 2.5 mL pyridine. The mixture was cooled to 0 °C and stirred for 10 min. The obtained yellow solid was dissolved in 15 mL anhydrous THF and added to the mixture dropwise at 0 °C. The reaction was then heated to reflux for 12 h. The reaction was cooled to room temperature and the solvent was removed under reduced pressure. The residue was purified by silica column to yield probe **NAP-SCM** as white solid. ^{1}H NMR (600 MHz, Chloroform-d) δ 9.12 (d, J = 8.6 Hz, 1H), 8.79 (d, J = 7.3 Hz, 1H), 8.58 (d, J = 7.7 Hz, 1H), 8.31 (d, J = 7.7 Hz, 1H), 8.07 (t, J = 8.0 Hz, 1H), 7.62 (d, J = 9.6 Hz, 1H), 7.40 (d, J = 8.5 Hz, 1H), 6.98 (dd, J = 8.6, 2.3 Hz, 1H), 6.71 (d, J = 2.3 Hz, 1H), 6.38 (d, J = 9.5 Hz, 1H), 4.19 (t, J = 7.7 Hz, 2H), 1.73 (h, J = 7.6 Hz, 2H), 1.46 (h, J = 7.4 Hz, 2H), 0.98 (t, J = 7.4 Hz, 3H); ^{13}C NMR (150 MHz, Chloroform-d) δ 162.99, 162.48, 159.38, 154.31, 151.00, 142.27, 135.30, 132.37, 131.14, 130.60, 130.50, 129.84, 129.11, 128.93, 128.49, 127.07, 123.57, 118.50, 118.02, 117.09, 110.45, 40.70, 30.07, 20.33, 13.79. HRMS (ESI) calcd. for $C_{25}H_{18}NSO_7^+$ [M + H^+] 478.0960, found 478.0962.

3. Results and discussion

3.1. Probe design and synthesis

In order to evaluate the suggestion proposed in Scheme 1, probe **NAP-SCM** was synthesized according to the previous literature [42]. The commercially available 4-potassiosulfo-1,8-naphthalenedicarboxylic anhydride was converted into *N*-butyl-1,8-naphthalimide **NAP-SOK**. The condensation of **NAP-SCM** with 7-hydroxylcoumarin in the presence of $SOCl_2$ could produce probe **NAP-SCM** finally (Scheme 2). The structure of **NAP-SCM** was characterized by ^1H NMR, ^{13}C NMR and ESI-HRMS (Figs. S1–S3).

3.2. The spectroscopic properties and TD-DFT calculations

The capability of probe **NAP-SCM** to detect $O_2^{\cdot-}$ was first investigated under simulated physiological conditions (1.0 mM PBS buffer, pH = 7.4). As the results shown in Fig. 1a, the probe **NAP-SCM** is non-fluorescent in the absence of $O_2^{\cdot-}$ by the incorporation of 1,8-naphthalimidesulfonyl unit. With the increasing concentrations of $O_2^{\cdot-}$ added in a solution of **NAP-SCM** (10 μM in PBS buffer), the emission band peaked at 454 nm is dramatically enhanced. The intensity arrived the maximum when the concentration of $O_2^{\cdot-}$ is above 150 μM, which corresponds to a fluorescence enhancement of about 55 folds (Fig. 1b). The fluorescence intensity at 454 nm displayed an excellent linear relationship (R^2 = 0.9915) towards the concentrations of $O_2^{\cdot-}$ ranging from 0 to 25 μM. The result displayed that probe **NAP-SCM** is well suited for quantitatively monitoring $O_2^{\cdot-}$. The detection limit was calculated to be as low as 78 nM according to the 3δ/k criterion, indicating the high sensitivity of probe **NAP-SCM** for $O_2^{\cdot-}$ detection (Fig. 1b insert). Furthermore, the slight increasing of UV absorption band centered at 340 nm takes place in the correspondence with the occurrence of the response for $O_2^{\cdot-}$ (Fig. S4).

The time-dependent density functional theory (TD-DFT) calculations were then conducted in order to shed light on the fluorescent change. As shown in Fig. S5, the highest occupied molecular orbital (HOMO) was mainly located on the coumarin moiety while the lowest unoccupied molecular orbital (LUMO) mainly dispersed on the naphthalimidesulfonyl unit in the probe **NAP-SCM**. The frontier orbitals of the fluorophore (**HYCA**) and the masking moiety (**NAP-SOH**) were also illustrated in Fig. S6. The empty orbital (LUMO) of **NAP-SOH** located between the HOMO and LUMO levels of **HYCA**, which facilitated the photoinduced electron transfer (PET) process and consequently switched off the fluorescence of fluorophore in the probe [43].

3.3. Selectivity of NAP-SCM towards $O_2^{\cdot-}$ and pH tolerance

The good specificity towards the desired target is another important component for an ideal probe. Therefore, the fluorescent response of probe **NAP-SCM** to a variety of bioanalytes, including ROS ($^1O_2$, HOCl, H_2O_2), RNS (NO_2^-, NO•, HNO, $ONOO^{\bullet-}$), RSS (H_2S, cysteine (Cys), homocysteine (Hcy), glutathione (GSH)) and other relative species such as ascorbic acid (AA), ferrous ion (Fe^{2+}) and 1,4-hydroquinone (HQ) were explored (Fig. 2). In contrast to the significant fluorescent enhancement (~55 folds) caused by $O_2^{\cdot-}$, probe **NAP-SCM** suffered hardly change in the presence of other analytes, which indicate **NAP-**

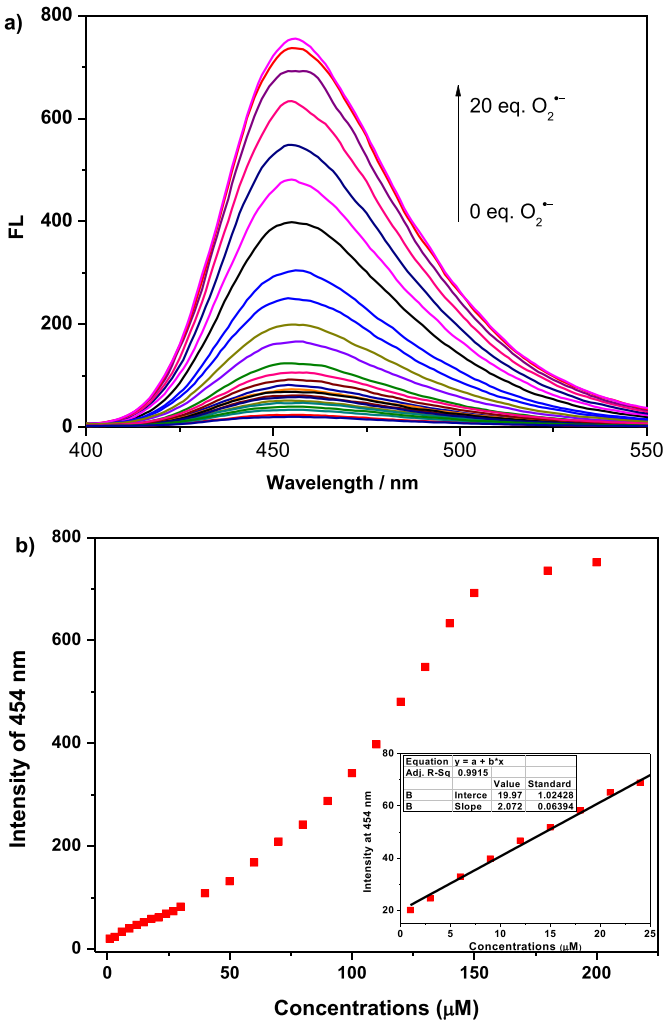

Fig. 1. a) Fluorescence spectra of probe **NAP-SCM** (10 μM) upon addition of different amounts of $O_2^{\cdot-}$ (0–200 μM) in PBS buffer (1.0 mM, pH 7.4); b) Fluorescence response of probe **NAP-SCM** (10 μM) at 454 nm to different concentrations of $O_2^{\cdot-}$ (0–200 μM); b) insert: The linear relationship between fluorescence intensity at 454 nm and $O_2^{\cdot-}$. Spectra were recorded after incubation with different concentrations of $O_2^{\cdot-}$ for 20 min λ_{ex} = 390 nm, λ_{em} = 454 nm. Slits: 3/5 nm.

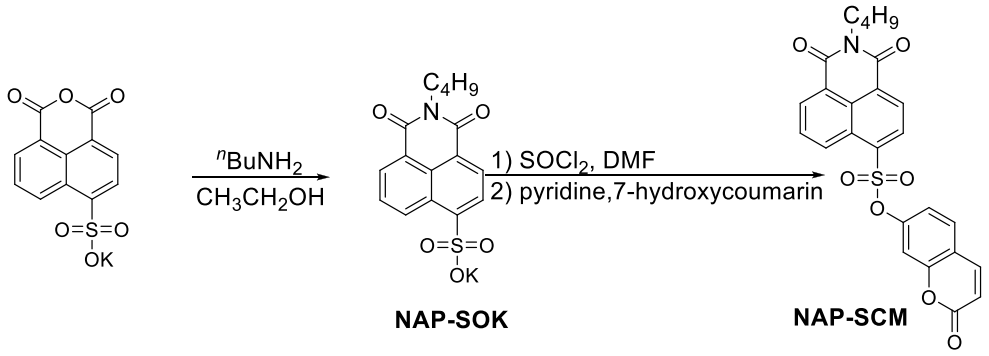

Scheme 2. Route for synthesis of probe **NAP-SCM**.

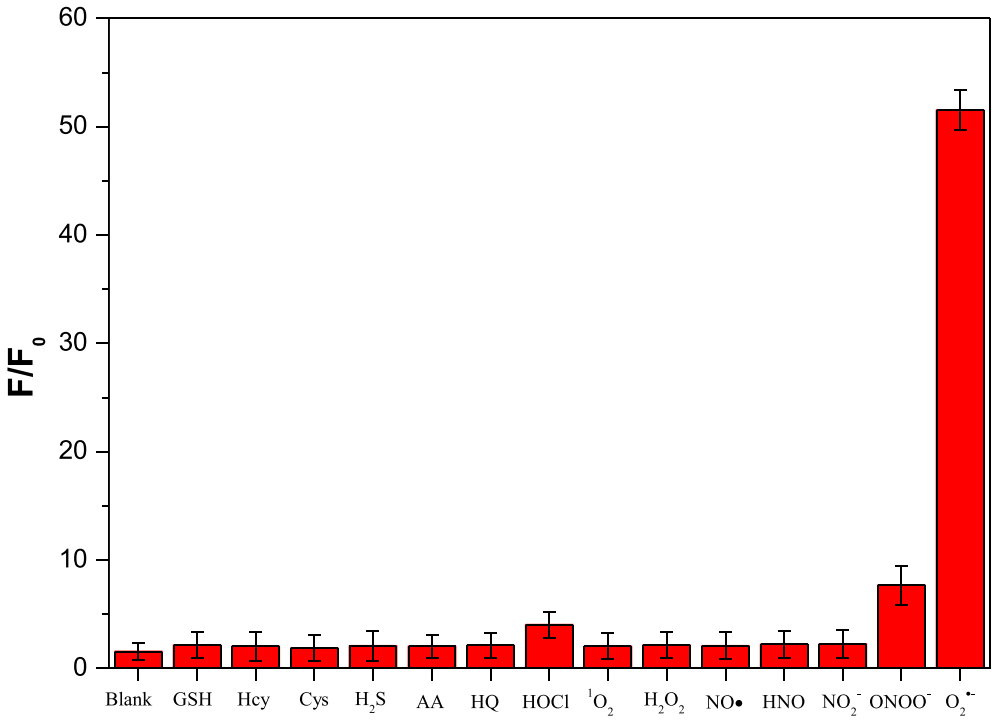

Fig. 2. Relative fluorescence intensities of probe **NAP-SCM** in the absence and presence of $O_2^{\cdot-}$ and other reactive analytes (200 μM) in PBS buffer (1.0 mM, pH 7.4).

SCM is highly specific for $O_2^{\cdot-}$.

In addition, the pH-dependent fluorescent response of **NAP-SCM** for $O_2^{\cdot-}$ is examined under different pH buffers in order to study the further biological applicability. As shown in Fig. 3, **NAP-SCM** displayed superior stability over the pH 3–9. With the addition of $O_2^{\cdot-}$ to the **NAP-SCM** containing solutions at pH value ranging from 4 to 11, the significant enhancement could be witnessed. This broad pH tolerance revealed **NAP-SCM** possesses the potential applications in biochemical system.

3.4. The kinetic study and sensing mechanism of NAP-SCM for detection of $O_2^{\cdot-}$

Considering the rapid metabolism nature of $O_2^{\cdot-}$ in the living systems,

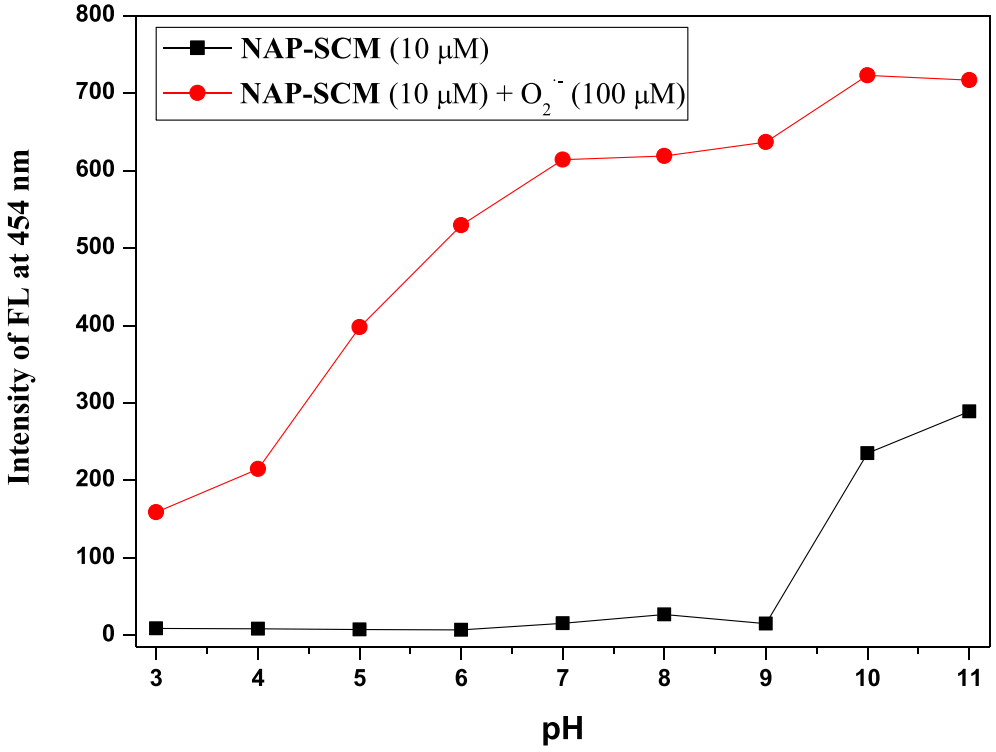

Fig. 3. Fluorescence intensity of probe **NAP-SCM** (10 μM) at 454 nm under different pH values in the absence and the presence of 15 equiv. of $O_2^{\cdot-}$ in PBS buffer (1.0 mM, pH = 7.4). Spectra were recorded after incubation of $O_2^{\cdot-}$ for 20 min.

the rapid reaction rate is essential for the biological applications. Thus, the rate constant for the reaction of probe **NAP-SCM** and $O_2^{\cdot-}$ was investigated using the time-dependent fluorescence change. As the results shown in Fig. 4, the addition of 10 equiv. of $O_2^{\cdot-}$ leads to a rapid and dramatic increasing of fluorescence intensity at 454 nm and the maximum intensity was achieved after about 5 min. The results demonstrated that response of probe **NAP-SCM** with $O_2^{\cdot-}$ is rapid and the product of probe **NAP-SCM** with $O_2^{\cdot-}$ possesses the excellent photostability under visible light. The pseudo-first-order rate constant (k_{obs}) for the reaction of probe **NAP-SCM** and $O_2^{\cdot-}$ is estimated to be 1.0 × 10^{-2} s^{-1} on the basis of the kinetic data (Fig. 4 insert).

According to well reported protection-deprotection processes [32–34], the sensing mechanism proposed in Scheme 1 is verified by monitoring the PBS buffer solution which contains the mixture of probe **NAP-SCM** (10 μM) and superoxide radical anion (100 μM) under high-resolution mass spectrometry (HRMS). As the mass spectrum shown in Fig. S7, the new peaks arised at 161.0250 (*m/z*) and 332.0613 (*m/z*) are well matched with the formation of the main product **HYCA** (calcd *m/z* 161.0244 for $C_9H_5O_3$) and **NAP-SOH** (calcd *m/z* 332.0598 for $C_{16}H_{14}NSO_5$), respectively. The peak located at 478.0974 is consistent with the remained probe **NAP-SCM**. In order to further confirm the reaction mechanism, the ^{1}H NMR titration experiment was conducted. As the result shown in Fig. S8, the addition of 5.0 equiv of KO_2 (dissolved in DMSO d_6) led to the weakening of signals (H_{a1} at 6.46 ppm, H_{b1} at 6.88 ppm, H_{c1} at 7.13 ppm and H_{d1} at 7.63 ppm) relevant to the aromatic protons of coumarin moiety in probe **NAP-SCM**. Meanwhile, the new upfield peaks at about 5.30 (H_{a2}), 5.94 (H_{b2}), 5.68 (H_{c2}) and 7.41 ppm (H_{d2}) were witnessed, which attributed to the self-cleavage triggered by $O_2^{\cdot-}$. Moreover, the fluorescent spectrum of the mixture following the reaction of **NAP-SCM** with $O_2^{\cdot-}$ is well matched the fluorescent spectrum of 7-hydroxycoumarin (**HYCA)** which has been reported previously [44,45].

3.5. Imaging endogenous $O_2^{\cdot-}$ in RAW 264.7 cells

Encouraged by good performance in the simulated physiological conditions, the potential applications of probe **NAP-SCM** in biological systems were further examined. RAW 264.7 macrophages were utilized as a bioassay model in result from its ability to generate ROS and RNS in immunological and inflammatory processes. Initially, the survival rate of RAW 264.7 macrophages under different amounts of **NAP-SCM** was employed to estimate the cytotoxicity. As the results shown in Fig. S9, over 85% RAW 264.7 cells could well survived in the concentrations of **NAP-SCM** from 0 to 20 μM, indicating probe **NAP-SCM** possessed good bio-compatibility and negligible cytotoxicity. Subsequently, the capability of probe **NAP-SCM** to monitor $O_2^{\cdot-}$ inside cells was employed. According to the previous report, the cellular endogenous $O_2^{\cdot-}$ could be generated by phorbol myristate acetate (PMA) or lipopolysaccharide (LPS) [46]. As can be seen by viewing Fig. 5a, when RAW 264.7 macrophages were loaded with probe **NAP-SCM** (10 μM) at 37 °C for 30 min, only faint intracellular background fluorescence could be observed under confocal microscopy. In sharp contrast, when RAW 264.7 macrophages were pretreated with PMA (1 μg/mL) for 12 h, and then were incubated with probe **NAP-SCM** for 30 min, a notable enhancement in fluorescence images was observed (Fig. 5b). Similarly, the distinct blue fluorescence was observed within cells after treated with LPS (5 μg/mL) (Fig. 5c). To further verify the specificity of probe **NAP-SCM** to measure the endogenous $O_2^{\cdot-}$, the PMA-stimulated or LPS-stimulated RAW264.7 macrophages were pre-treated with Tiron (1,2-dihydroxy-3,5-benzenedisulfonic acid disodium salt), a common used cell-permeable $O_2^{\cdot-}$ scavenger, for 1 h and then incubated with probe **NAP-SCM** for 30 min [47]. As the results in Fig. 5d and e, the bright cellular fluorescence is significantly attenuated under confocal microscopy. The combined results demonstrate that **NAP-SCM** can be utilized for specific and sensitive imaging of endogenous $O_2^{\cdot-}$ in live cells.

3.6. Imaging endogenous $O_2^{\cdot-}$ in live zebrafish

Moreover, we also investigated the capability of tracking endogenous $O_2^{\cdot-}$ in live zebrafish. As the results shown in Fig. 6, when zebrafish was incubated with probe **NAP-SCM**, a very weak fluorescence was observed (Fig. 6b). The distinct fluorescence distribution was then observed after zebrafish was pre-treated with PMA (Fig. 6c). In contrast, the fluorescence was significantly diminished when Tiron was added

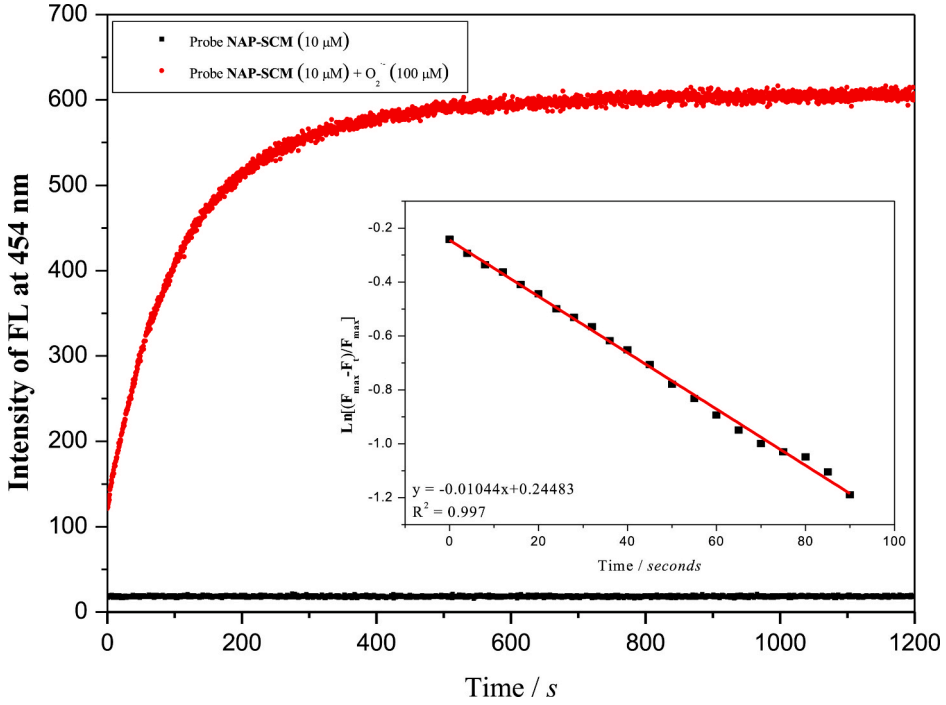

Fig. 4. Time course experiment of probe **NAP-SCM** (10 μM) with $O_2^{\cdot-}$ (100 μM) in PBS buffer (1.0 mM, pH = 7.4). Insert: Pseudo first-order kinetic plot of **NAP-SCM** (10 μM) with the addition of 10 equiv. of $O_2^{\cdot-}$.

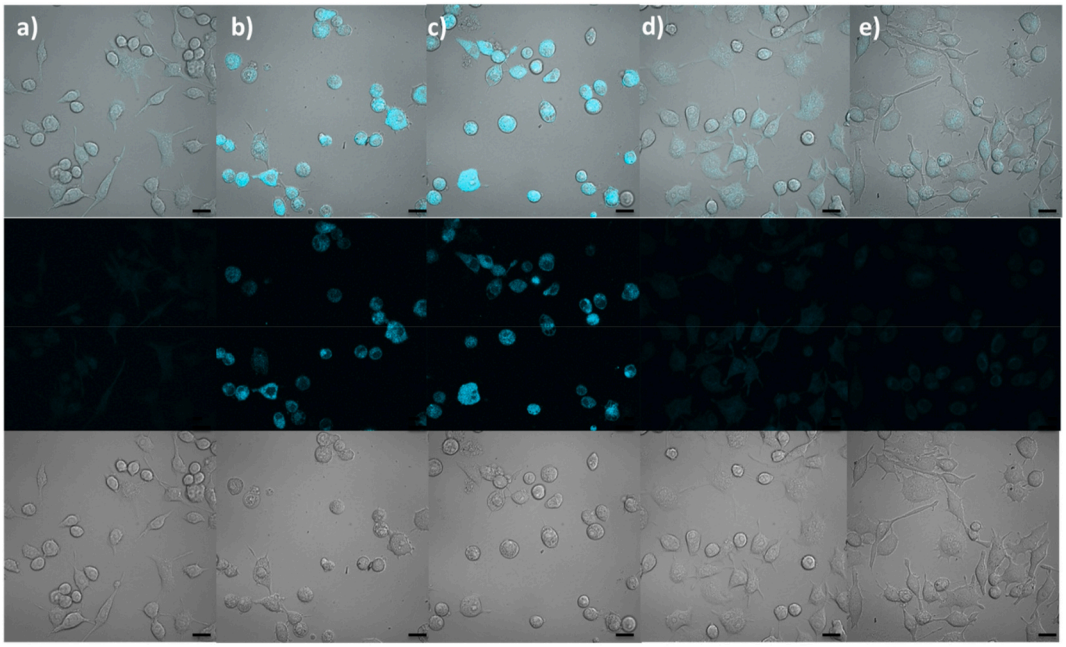

Fig. 5. Detection of superoxide radical anion produced by an immune reaction in the macrophage RAW 264.7 cells. RAW 264.7 cells were treated with (a) 0; (b) 1 μg/mL PMA for 12 h; (c) 5 μg/mL LPS for 8 h; (d) RAW 264.7 cells were pre-treated with Tiron (100 μM) for 1 h, then 1 μg/mL PMA for 12 h; (e) RAW 264.7 cells were pre-treated with Tiron (100 μM) for 1 h, then 5 μg/mL LPS for 8 h. The cells were incubated with 10 μM probe **NAP-SCM** for 30 min and washed with DPBS and imaged by confocal microscopy; (d) bar graphs about mean fluorescent intensities in (a–c); λ_{ex} 405 nm/λ_{em} 465–495 nm. Scale bar: 10 μm.

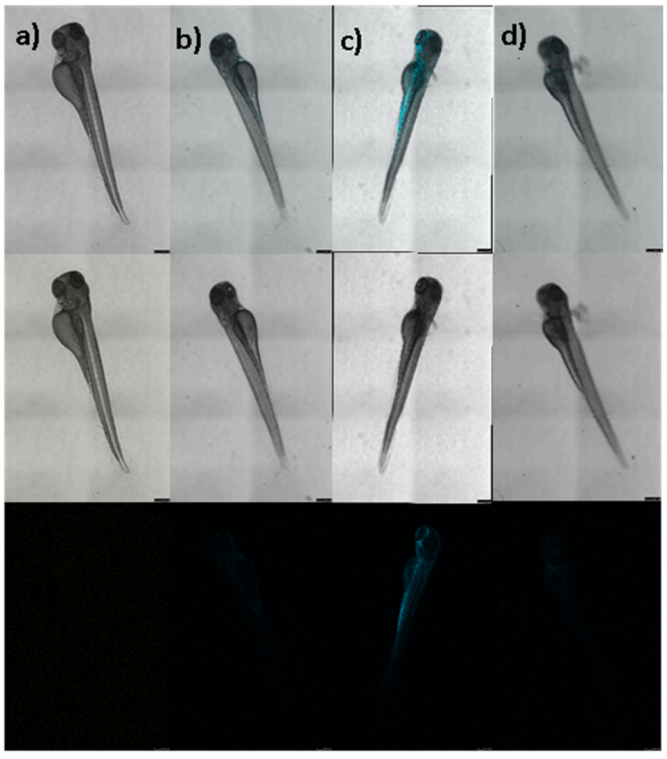

Fig. 6. Confocal imaging of endogenous $O_2^{\bullet-}$ in 72 h post-fertilization zebrafish embryos. (a) Blank; (b) Zebrafish was incubated with probe **NAP-SCM** (10 μM) for 30 min; (c) Zebrafish briefly challenged with PMA (1 μg/mL) for 12 h after preloaded with probe **NAP-SCM** (10 μM) for 30 min; (d) Zebrafish initially stimulated with PMA (1 μg/mL) for 30 min and treated with Tiron (100 μM) for 1 h was loaded with probe **NAP-SCM** (10 μM) for 30 min λ_{ex} 405 nm/λ_{em} 465–495 nm. Scale bar = 10 μm.

after the treatment of PMA (Fig. 6d). These results indicate that **NAP-SCM** can be utilized as a promising fluorescence imaging agent for the detection of $O_2^{\bullet-}$ in live animals.

4. Conclusion

In summary, a novel non-redox strategy based fluorescence probe **NAP-SCM** for the measurement of $O_2^{\bullet-}$ is designed and synthesized utilizing coumarin as the fluorescent platform and 1,8-naphthalimidesulfonyl as the masking moiety. Probe **NAP-SCM** displayed excellent detection performance for $O_2^{\bullet-}$ in vitro including the good specificity to $O_2^{\bullet-}$ over other reactive species, the rapid response, the high light stability, the high sensitivity with the detection limit as low as 78 nM, the good linearship in a wide range of $O_2^{\bullet-}$ concentrations and a wide pH tolerance. Furthermore, the biologically potential of probe **NAP-SCM** is demonstrated by its low cytotoxicity, good bio-compatibility and the capability to monitor the endogenous $O_2^{\bullet-}$ in RAW 264.7 cells and live zebrafish with high specificity. Collectively, the favorable observations in this investigation demonstrate the high practical value of probe **NAP-SCM** for elucidating the biological roles of $O_2^{\bullet-}$ in future studies.

CRediT authorship contribution statement

Liyan Chen: Formal analysis, Investigation, Writing – original draft, Writing – review & editing. **Xin Lu:** Formal analysis, Investigation, NMR experiment. **Fengping Xiao:** Spectroscopic experiments. **Di Wu:** Supervision, Writing – review & editing, All authors discussed the results and contributed to the final manuscript.

Declaration of competing interest

The authors declare that they have no known competing financial interests or personal relationships that could have appeared to influence the work reported in this paper.

Acknowledgments

This work was supported by the National Natural Science Foundation of China (NSFC, 22007034). We thank the researchers from Central China Normal University Analytical and Testing Center for their assistance with data analysis.

Appendix A. Supplementary data

Supplementary data to this article can be found online at https://doi.org/10.1016/j.dyepig.2021.109614.

References

[1] Finkel T, Holbrook NJ. Oxidants, oxidative stress and the biology of aging. Nature 2000;408:239–47.
[2] Branzk N, Lubojemska A, Hardison SE, Wang Q, Gutierrez MG, Brown GD, Papayannopoulos V. Neutrophils sense microbe size and selectively release neutrophil extracellular traps in response to large pathogens. Nat Immunol 2014; 15:1017–25.
[3] Strowig T, Henao-Mejia J, Elinav E, Flavell R. Inflammasomes in health and disease. Nature 2012;481:278–86.
[4] Turrens JF. Mitochondrial formation of reactive oxygen species. J Physiol 2003; 552:335–44.
[5] Brand MD. The sites and topology of mitochondrial superoxide production. Exp Gerontol 2010;45:466–72.
[6] Gao JJ, Xu KH, Tang B, Yin LL, Yang GW, An LG. Selective detection of superoxide anion radicals generated from macrophages by using a novel fluorescent probe. FEBS J 2007;274:1725–33.
[7] Bokkon I. Recognition of functional roles of free radicals. Curr Neuropharmacol 2012;10:287–8.
[8] Rahman MA, Kothalam A, Choe ES, Won MS, Shim YB. Stability and sensitivity enhanced electrochemical in vivo superoxide microbiosensor based on covalently co-immobilized lipid and cytochrome. Anal Chem 2012;84:6654–60.
[9] Kundu K, Knight SF, Willett N, Lee S, Taylor WR, Murthy N. Hydrocyanines: a class of fluorescent sensors that can image reactive oxygen species in cell culture, tissue and in vivo. Angew Chem Int Ed 2009;48:299–303.
[10] Zhang X, Yu L, Xu H. Lysosome calcium in ROS regulation of autophagy. Autophagy 2016;12:1954–5.
[11] Chaudhury S, Sarkar PK. Stimulation of tubulin synthesis by thyroid hormone in the developing rat brain. Biochim Biophys Acta Mol Cell Res 1983;763:93–8.
[12] Kozumbo WJ, Trush MA, Kensler TW. Are free radicals involved in tumor promotion. Chem Biol Interact 1985;54:199–207.
[13] Abbas K, Hardy M, Poulhes F, Karoui H, Tordo P, Ouari O. Detection of superoxide production in stimulated and unstimulated living cells using new cyclic nitrone spin traps. Free Radic Biol Med 2014;71:281–90.
[14] Yasui H, Sakurai H. Chemiluminescent detection and imaging of reactive oxygen species in live mouse skin exposed to UVA. Biochem Biophys Res Commun 2000; 269:131–6.
[15] Cadet J, Cadet J, Douki T, Gasparutto D, Ravanat JL. Oxidative damage to DNA: formation, measurement and biochemical features. Mutat Res Fund Mol Mech Mutagen 2003;531:5–23.
[16] Yin H, Xu L, Porter NA. Free radical lipid peroxidation: mechanisms and analysis. Chem Rev 2011;111:5944–72.
[17] Liu H, Zhang L, Chen J, Zhai Y, Zeng Y, Li L. A novel functional imidazole fluorescent ionic liquid: simple and efficient fluorescent probes for superoxide anion radicals. Anal Bioanal Chem 2013;405:9563–70.
[18] Zhang J, Chai K, He XP, Kim HJ, Yoon J, Tian H. Fluorogenic probes for disease-relevant enzymes. Chem Soc Rev 2019;48:683–722.
[19] Cheng HB, Zhang YM, Liu Y, Yoon Y. Turn-On supramolecular host-guest nanosystems as theranostics for cancer. Chem 2019;5:553–74.
[20] Sun W, Guo S, Hu C, Fan J, Peng X. Recent development of chemosensors based on cyanine platforms. Chem Rev 2016;116:7768–817.
[21] Vendrell M, Zhai D, Er JC, Chang YT. Combinatorial strategies in fluorescent probe development. Chem Rev 2012;112:4391–420.
[22] Li X, Gao X, Shi W, Ma H. Design strategies for water-soluble small molecular chromogenic and fluorogenic probes. Chem Rev 2014;114:590–659.
[23] Zielonka J, Kalyanaraman B. Hydroethidine- and MitoSOX-derived red fluorescence is not a reliable indicator of intracellular superoxide formation: another inconvenient truth. Free Radic Biol Med 2010;48:983–1001.
[24] Dikalov S, Griendling KK, Harrison DG. Measurement of reactive oxygen species in cardiovascular studies. Hypertension 2007;49:717–27.
[25] Robinson KM, Janes MS, Pehar M, Monette JS, Ross MF, Hagen TM, Murphy MP, Beckman JS. Selective fluorescent imaging of superoxide in vivo using ethidium-based probes. Proc Natl Acad Sci U S A 2006;103:15038–43.
[26] Zielonka J, Kalyanaraman B. Hydroethidine-and MitoSOX-derived red fluorescence is not a reliable indicator of intracellular superoxide formation: another inconvenient truth. Free Radical Biol Med 2010;48:983–1001.
[27] Maeda H, Yamamoto K, Nomura Y, Kohno I, Hafsi L, Ueda N, Yoshida S, Fukuda M, Fukuyasu Y, Yamauchi Y, Itoh N. A design of fluorescent probes for superoxide based on a nonredox mechanism. J Am Chem Soc 2005;127:68–9.
[28] Maeda H, Fukuyasu Y, Yoshida S, Fukuda M, Saeki K, Matsuno H, Yamauchi Y, Yoshida K, Hirata K, Miyamoto K. Fluorescent probes for hydrogen peroxide based on a non-oxidative mechanism. Angew Chem Int Ed 2004;43:2389–91.
[29] Maeda H, Matsuno H, Ushida M, Katayama K, Saeki K, Itoh N. 2,4-Dinitrobenzenesulfonyl fluoresceins as fluorescent alternatives to Ellman's reagent in thiol-quantification enzyme assays. Angew Chem Int Ed 2005;44:2922–5.
[30] Maeda H, Katayama K, Matsuno H, Uno T. 3′-(2,4-Dinitrobenzenesulfonyl)- 2′,7′-dimethylfluorescein as a fluorescent probe for selenols. Angew Chem Int Ed 2006; 45:1803–10.
[31] Maeda H, Yamamoto K, Kohno I, Hafsi L, Itoh N, Nakagawa S, Kanagawa N, Suzuki K, Uno T. Design of a practical fluorescent probe for superoxide based on protection-deprotection chemistry of fluoresceins with benzenesulfonyl protecting groups. Chem Eur J 2007;13:1946–54.
[32] Hu JJ, Wong NK, Ye S, Chen X, Lu MY, Zhao AQ, Guo Y, Ma ACH, Leung AYH, Shen J, Yang D. Fluorescent Probe HKSOX-1 for imaging and detection of endogenous superoxide in live cells and in vivo. J Am Chem Soc 2015;137: 6837–43.
[33] Lu D, Zhou L, Wang R, Zhang X-B, He L, Zhang J, Hu X, Tan W. A two-photon fluorescent probe for endogenous superoxide anion radical detection and imaging in living cells and tissues. Sensor Actuator B 2017;250:259–66.
[34] Ma H, Ma Y, Liu Q, Lin W. A two-photon fluorescent probe with lysosome targetability for imaging endogenous superoxide anion in living cells, zebrafish and pneumonia tissue. Sensor Actuator B Chem 2021;332:129523.
[35] Zhang J, Li C, Zhang R, Zhang F, Liu W, Liu X, Lee SM-Y, Zhang H. A phosphinate-based near-infrared fluorescence probe for imaging the superoxide radical anion in vitro and in vivo. Chem Commun 2016;52:2679–82.
[36] Gao X, Feng G, Manghnani PN, Hu F, Jiang N, Liu J, Liu B, Sun JZ, Tang BZ. A two-channel responsive fluorescent probe with AIE characteristics and its application for selective imaging of superoxide anions in living cells. Chem Commun 2017;53: 1653–6.
[37] Xu K, Liu X, Tang B, Yang G, Yang Y, An L. Design of a phosphinate-based fluorescent probe for superoxide detection in mouse peritoneal macrophages. Chem Eur J 2007;13:1411–6.
[38] Wang J, Liu L, Xu W, Yang Z, Yan Y, Xie X, Wang Y, Yi T, Wang C, Hua J. Mitochondria-targeted ratiometric fluorescent probe based on diketopyrrolopyrrole for detecting and imaging of endogenous superoxide anion in vitro and in vivo. Anal Chem 2019;91:5786–93.
[39] Zhang Z, Fan J, Zhao Y, Kang Y, Du J, Peng X. Mitochondria-accessing ratiometric fluorescent probe for imaging endogenous superoxide anion in live cells and *Daphnia magna*. ACS Sens 2018;3:735–41.
[40] Chen L, Cho MK, Wu D, Kim HM, Yoon J. Two-Photon fluorescence probe for selective monitoring of superoxide in live cells and tissues. Anal Chem 2019;91: 14691–6.
[41] Reed JW, Ho HH, Jolly WL. Chemical syntheses with a quenched flow reactor: hydroxytrihydroborate and peroxynitrite. J Am Chem Soc 1974;96:1248–9.
[42] Cao M, Chen H, Chen D, Xu Z, Liu SH, Chen X, Yin J. Naphthalimide-based fluorescent probe for selectively and specifically detecting glutathione in the lysosomes of living cells. Chem Commun 2016;52:721–6.
[43] Ramón M-M, Sancenón F. Fluorogenic and chromogenic chemosensors and reagents for anions. Chem Rev 2003;103:4419–76.
[44] Iqbal PF, Bhat AR, Azam A. Antiamoebic coumarins from the root bark of Adina cordifolia and their new thiosemicarbazone derivatives. Eur J Med Chem 2009;44: 2252–9.
[45] Chakraborty M, Bardhan S, Saha SK, Panda AM. Effect of colloidal silica on the spectral behaviour of 7-hydroxycoumarin in aqueous medium. Spectrochim Acta 2012;97:722–7.
[46] Tyagi R, Tamura M, Burnham DN, Lambeth JD. Phorbol myristate acetate (PMA) augments chemoattractant-induced diglyceride generation in human neutrophils but inhibits phosphoinositide hydrolysis. Implications for the mechanism of PMA priming of the respiratory burst. J Biol Chem 1988;263:13191–8.
[47] Vaquero EC, Edderkaoui M, Pandol SJ, Gukovsky I, Gukovskaya AS. Reactive oxygen species produced by NAD(P)H oxidase inhibit apoptosis in pancreatic cancer cells. J Biol Chem 2004;279:34643–54.